

Neutrino-nucleon elastic scattering in presence of non-standard interactions: cross sections and nucleon polarizations

Ilma,^{1,*} M. Rafi Alam,^{1,†} L. Alvarez-Ruso,² M. Benitez Galan,³ I. Ruiz Simo,^{3,‡} and S. K. Singh¹

¹*Department of Physics, Aligarh Muslim University, Aligarh-202002, India*

²*Instituto de Física Corpuscular (IFIC), Consejo Superior de Investigaciones Científicas (CSIC) and Universidad de Valencia, E-46980 Paterna, Valencia, Spain*

³*Departamento de Física Atómica, Molecular y Nuclear and Instituto Carlos I de Física Teórica y Computacional, Universidad de Granada, E-18071 Granada, Spain*

New physics beyond the Standard Model (SM) may appear in the form of non-standard neutrino interactions (NSI). We have studied neutral current (anti)neutrino-nucleon scattering in presence of NSI. We obtain that in this scenario, nucleon matrix elements depend not only on the isovector axial nucleon form factor but also on the isoscalar one. For the axial form factors we consequently rely on the quark flavor decomposition performed by QCD simulations in the lattice (LQCD). We have examined cross sections and polarization observables. For the current bounds on diagonal muon flavor NSI couplings we find substantial deviations from the SM predictions in cross sections and transverse polarizations of the outgoing nucleons. In view of the progress in the precision of LQCD determinations of nucleon properties, modern measurements of neutral current (anti)neutrino-nucleon scattering will be in the position to discover or significantly constrain NSI.

I. INTRODUCTION

The Standard Model (SM) is a successful paradigm for understanding particle physics. In particular, it has proved capable of explaining a wide range of physical phenomena involving electroweak interactions. The SM assumes neutrinos of all flavors to be massless and the conservation of lepton flavors in neutrino interactions [1]. However, it has been established that neutrinos undergo flavor oscillations during their propagation, thus violating the lepton flavor conservation [2]. The phenomenon of neutrino oscillation further implies that neutrinos are not massless, and the mass states are nontrivial admixtures of flavor states. The theoretical models explaining this physics go beyond the SM and, below the weak scale, give rise to new types of neutrino interactions [3–6]. The subset of these generalized interactions involving only SM left(right)-handed (anti)neutrinos and Lorentz-invariant four-fermion terms built from vector and axial-vector operators is phenomenologically coined as non-standard interactions (NSI) [7–11].

Non-standard interactions are also categorized into two groups, Charged Current (CC) NSI and Neutral Current (NC) NSI, similar to standard weak interactions. Through matter effects, certain combinations of NC NSI can bias some of the mixing angles extracted from oscillation experiments (for a review see Ref. [12]). Moreover, besides measuring mixing parameters with unprecedented accuracy, the upcoming generation of neutrino experiments will be sensitive to yet-unknown neutrino parameters like the mass ordering and CP-violating phase. NSI can have an impact on the interpretations

of long baseline experiments regarding the CP violating phase [13–17]. Therefore, the study of NSI is crucial for accurately interpreting the results of neutrino experiments and understanding the fundamental properties of neutrinos.

Non-standard interactions can also modify the way neutrinos scatter on matter, potentially leading to deviations from the SM predictions. The NSI contribution to neutrino-electron cross sections has been studied and constrained using experimental data [18–21]. Upper limits for the NSI parameters in the quark sector have been obtained from neutrino-nucleus scattering data in the deep inelastic scattering regime probed at high energies [10, 21, 22]. Further constraints on vector NC NSI couplings can be extracted from measurements for neutrino-nucleus elastic scattering, as has already been done with COHERENT data [23–30]. The impact of NSI on neutrino-nucleon (quasi)elastic and inelastic cross sections and related observables is considerably less explored [31–33]. This is justified by the present uncertainties in the hadronic input and the lack of precise data which render the task of extracting information about NSI highly difficult. Nevertheless, the availability of new Lattice QCD (LQCD) determinations of the isovector nucleon axial form factor (see Ref. [34] and references therein) together with the prospects of modern experimental studies of neutrino-nucleon interactions [35, 36] following the novel extraction of $\bar{\nu}_\mu p \rightarrow \mu^+ n$ -proton cross section by the MINERvA experiment [37] provide motivations to explore this avenue. In fact, a recent analysis of these data obtained new confidence intervals for tensor and scalar interactions [33]. Furthermore, Ref. [38] finds that tensor and pseudoscalar interactions might enhance neutrino-nucleus CC quasielastic scattering cross sections on nuclei. Along these lines, the $n - \Lambda_c$ transition induced by ν_τ CC interactions in the presence of new physics has been recently examined [39], showing how results from LQCD help to explore the new physics

* ilmarafiq786@gmail.com

† rafi.alam.amu@gmail.com

‡ ruizsig@ugr.es

backed by the future experimental data.

In this work, we investigate the impact of NSI on(anti)neutrino-nucleon NC elastic (NCE) cross sections, improving and extending the study of Ref. [31], and explore their effects in spin-dependent observables for the first time in the NC case. In particular, we study the polarization of the outgoing nucleon in the presence of NSI. There is no doubt that polarization measurements are challenging, even more so in the case of neutrino interactions, but spin observables allow for a more detailed scrutiny of the dynamics in play, as shown in several theoretical studies. The polarization of the outgoing lepton in CC quasielastic and inelastic neutrino-nucleon and neutrino-nucleus scattering has been extensively investigated [40–48]. This polarization is relevant for the ν_τ appearance measurements [49]. The asymmetries arising from the polarization of target nucleon and outgoing nucleon and lepton are derived in Ref. [32] for CC quasielastic scattering in presence of generalized interactions. The polarization of hyperons produced in CC neutrino-nucleon scattering has also been studied [50, 51]. It has been found that T -violating interactions lead to hyperon polarizations perpendicular to the scattering plane. For weak pion production, the sensitivity of polarization asymmetries to details of the interaction, such as the relative phases between resonant and non-resonant amplitudes, has been addressed in Refs. [52, 53].

For our study, we adopt the formalism of Refs [54, 55], where the final-nucleon polarization in NCE and CC quasielastic neutrino-nucleon scattering was calculated. The critical difference resides on the fact that the motivation then was to obtain information about the axial and strange axial form factors of the nucleon from neutrino scattering observables. Instead, we assume that the required nonperturbative QCD input can be (now or in the near future) provided by LQCD with sufficient precision to render feasible the investigation of new physics in neutrino-nucleon elastic scattering with future experimental data. From this perspective, the present paper can be regarded as a generalization of Ref. [55] to the NSI scenario. It is organized as follows: in Sec. II the formalism is presented. We introduce NC neutrino interactions with quarks in presence of NSI, which are then used to derive the nucleon matrix elements. Our choice for the nucleon form factors and NSI couplings are given afterwards. Next we introduce the spin density matrix, the cross section and derive the polarization of the outgoing nucleon. Our numerical results are presented in Sec. III. We conclude afterwards in Sec. IV.

II. FORMALISM

A. Neutrino-quark NC interactions in the presence of NSI

Following the common notation in the literature (see for instance Ref. [56]), the effective four-fermion NC-NSI

Lagrangian is given by

$$\mathcal{L}_{\text{NSI}}^{\text{NC}} = -2\sqrt{2}G_F\epsilon_{ij}^{fX}\bar{\nu}^i\gamma_\mu P_L\nu^j\bar{f}\gamma^\mu P_X f, \quad (1)$$

in terms of the projectors $P_{X=L,R} = (1 \mp \gamma_5)/2$; $i, j = e, \mu, \tau$ are neutrino flavor indices; G_F is the Fermi constant. In general f denotes lepton or quark fields. The present study is restricted to neutrino interactions with light quarks: $f = u, d, s$. Quark flavor conservation is implicit in the notation. Instead, the NC NSI couplings, denoted ϵ_{ij}^{fX} , can be flavor diagonal, $i = j$, or flavor changing, $i \neq j$, for the neutrinos.

In the limit where both NSI and SM NC interactions can be treated as contact ones, it is convenient to write an effective Lagrangian encompassing both SM and NSI

$$\mathcal{L}_{\text{SM+NSI}}^{\text{NC}} = -\frac{G_F}{\sqrt{2}}L_\mu^{ij}J_\mu^{ij} \quad (2)$$

with

$$L_\mu^{ij} = \bar{\nu}^i\gamma_\mu(1 - \gamma_5)\nu^j, \quad (3)$$

and

$$\begin{aligned} J_{ij}^\mu &= \delta_{ij} J_{\text{SM}}^\mu + (J_{ij}^\mu)_{\text{NSI}}, \\ J_{\text{SM}}^\mu &= \bar{u}\gamma^\mu \left[\frac{1}{2} - \left(\frac{2}{3}\right) 2s_w^2 - \frac{1}{2}\gamma_5 \right] u \\ &\quad + \bar{d}\gamma^\mu \left[-\frac{1}{2} - \left(-\frac{1}{3}\right) 2s_w^2 + \frac{1}{2}\gamma_5 \right] d \\ &\quad + \bar{s}\gamma^\mu \left[-\frac{1}{2} - \left(-\frac{1}{3}\right) 2s_w^2 + \frac{1}{2}\gamma_5 \right] s, \\ (J_{ij}^\mu)_{\text{NSI}} &= \bar{u}\gamma^\mu (\epsilon_{ij}^{uV} - \epsilon_{ij}^{uA}\gamma_5) u \\ &\quad + \bar{d}\gamma^\mu (\epsilon_{ij}^{dV} - \epsilon_{ij}^{dA}\gamma_5) d \\ &\quad + \bar{s}\gamma^\mu (\epsilon_{ij}^{sV} - \epsilon_{ij}^{sA}\gamma_5) s, \end{aligned} \quad (4)$$

where we have explicitly split the contribution of the quarks NC into the SM lepton-flavor diagonal current, and the, in general, non flavor diagonal NSI NC. In eqs. (4) u, d and s denote the spinor fields of the corresponding quark flavors; $\epsilon^{V,A} = \epsilon^L \pm \epsilon^R$ and $s_w \equiv \sin \theta_w$, where θ_w is the weak mixing angle.

B. Neutrino-nucleon NC interactions in presence of NSI

The (anti-)neutrino induced NCE scattering processes are:

$$\bar{\nu}^{(-)}(k, 0) + N(p, M) \rightarrow \bar{\nu}^{(-)}(k', 0) + N(p', M), \quad (5)$$

where $N(\equiv p, n)$ stands for the nucleon, and the corresponding four momenta with their masses are given in parentheses. The scattering amplitude is given by,

$$\mathcal{M} = \frac{G_F}{\sqrt{2}}l_\mu^{ij} \langle N | J_\mu^{ij} | N \rangle \quad (6)$$

where

$$l_{\mu}^{ij} = \bar{u}^i(k')\gamma_{\mu}(1 - \gamma_5)u^j(k) \quad (7)$$

or

$$l_{\mu}^{ij} = \bar{v}^j(k)\gamma_{\mu}(1 - \gamma_5)v^i(k') \quad (8)$$

for neutrinos or antineutrinos, respectively; $u, v(k)$ denote spinors in momentum space. Assuming isospin symmetry ($m_u = m_d \neq m_s$) and neglecting radiative corrections¹, the nucleon matrix element

$$\langle N | J_{ij}^{\mu} | N \rangle = \bar{u}(p')\Gamma_{ij}^{\mu}u(p) \quad (9)$$

can be expressed in terms of vector and axial-vector form factors (FF):

$$\begin{aligned} \Gamma^{\mu} &= V^{\mu} - A^{\mu}, \\ V^{\mu} &\equiv \tilde{F}_1^{(N)}(Q^2)\gamma^{\mu} + i\frac{\tilde{F}_2^{(N)}(Q^2)}{2M}\sigma^{\mu\nu}q_{\nu}, \\ A^{\mu} &\equiv \tilde{F}_A^{(N)}(Q^2)\gamma^{\mu}\gamma_5 + \frac{\tilde{F}_P^{(N)}(Q^2)}{M}q^{\mu}\gamma_5, \end{aligned} \quad (10)$$

which depend upon the four-momentum transfer squared $Q^2 = -(k-k')^2$. Lepton flavor indices have been dropped to alleviate the notation. In the observable quantities, the contribution of \tilde{F}_P is always proportional to powers of the outgoing neutrino mass and, therefore, negligible. It is actually exactly zero in the massless neutrino approximation adopted here and disregarded from now on. Owing to isospin symmetry, the FF introduced in Eq. (10) can be related to the isovector and isoscalar vector and axial vector FF. Furthermore, the vector ones can be written in terms of the electromagnetic FF of protons and neutrons $F_{1,2}^{(p,n)}$. In the presence of NSI, one obtains that

$$\begin{aligned} \tilde{F}_{1,2}^{(p,n)} &= \left[\left(\frac{1}{2} - 2s_w^2 \right) \delta_{ij} + 2\epsilon_{ij}^{uV} + \epsilon_{ij}^{dV} \right] F_{1,2}^{(p,n)} \\ &+ \left(-\frac{1}{2}\delta_{ij} + 2\epsilon_{ij}^{dV} + \epsilon_{ij}^{uV} \right) F_{1,2}^{(n,p)} \\ &+ \left(-\frac{1}{2}\delta_{ij} + \epsilon_{ij}^{sV} \right) F_{1,2}^s, \\ \tilde{F}_A^{(p,n)} &= \pm \frac{1}{2} (\delta_{ij} + \epsilon_{ij}^{uA} - \epsilon_{ij}^{dA}) F_A^{iv} \\ &+ \frac{1}{2} (\epsilon_{ij}^{uA} + \epsilon_{ij}^{dA}) F_A^{is} \\ &+ \left(-\frac{1}{2}\delta_{ij} + \epsilon_{ij}^{sA} \right) F_A^s. \end{aligned} \quad (11)$$

In this way, the NSI contributions to the (anti)neutrino-nucleon cross sections are shaped by the well defined nucleon FF, which can be obtained from experiment and/or LQCD.²

Remarkably, in presence of NSI, the nucleon NC matrix element depends not only on the standard axial isovector FF, F_A^{iv} :

$$\begin{aligned} \langle p, n | (\bar{u}\gamma^{\mu}\gamma_5u - \bar{d}\gamma^{\mu}\gamma_5d) | p, n \rangle &\equiv \\ \pm \bar{u}(p') \left[F_A^{iv}(Q^2)\gamma^{\mu}\gamma_5 + \frac{F_P^{iv}(Q^2)}{M}q^{\mu}\gamma_5 \right] u(p) \end{aligned} \quad (12)$$

but also on the axial vector isoscalar FF, F_A^{is} :

$$\begin{aligned} \langle p, n | (\bar{u}\gamma^{\mu}\gamma_5u + \bar{d}\gamma^{\mu}\gamma_5d) | p, n \rangle &\equiv \\ \bar{u}(p') \left[F_A^{is}(Q^2)\gamma^{\mu}\gamma_5 + \frac{F_P^{is}(Q^2)}{M}q^{\mu}\gamma_5 \right] u(p), \end{aligned} \quad (13)$$

not probed by SM electroweak interactions.

C. Form factors

Assuming there is no sizable new physics in electron scattering, one can take the electromagnetic FFs $F_{1,2}^{(p,n)}$ determined by the electron scattering and parameterized using experimental data. In fact, here we adopt standard parametrizations presented in Appendix A. The non-zero contribution due to the strange quark-sea in the nucleon leads to the strange vector ($F_{1,2}^s$) and axial (F_A^s) FF [59]. For the strange vector FF, we adopt the parametrization given in Ref. [60],

$$\begin{aligned} F_1^s(Q^2) &= -\frac{1}{6}\langle r_s^2 \rangle Q^2 F(Q^2) \\ F_2^s(Q^2) &= \mu_s F(Q^2), \end{aligned} \quad (14)$$

where $\langle r_s^2 \rangle$ is the mean-squared strange radius of the nucleon and μ_s is the strange magnetic moment. The $\langle r_s^2 \rangle$ can be further expressed in terms of the mean-squared strange charge radius, $\langle r_E^2 \rangle^s$, and μ_s as

$$\langle r_s^2 \rangle = \langle r_E^2 \rangle^s - \frac{3}{2} \frac{\mu_s}{M^2}. \quad (15)$$

A modified dipole form factor

$$F(Q^2) = \left(1 + \frac{Q^2}{4M^2} \right)^{-1} \left(1 + \frac{Q^2}{m_v^2} \right)^{-2} \quad (16)$$

is taken for the Q^2 dependence. The dipole mass, m_v , can be related to $\langle r_E^2 \rangle^s$ and the strange magnetic radius $\langle r_M^2 \rangle^s$ as³

$$m_v^2 = 12\mu_s (\langle r_M^2 \rangle^s - \langle r_E^2 \rangle^s)^{-1}. \quad (17)$$

¹ QED radiative corrections for CC neutrino-nucleon quasielastic scattering have been recently calculated in Refs. [57, 58].

² There is no need to introduce ad-hoc Q^2 dependent FF as in Ref. [31].

³ The feature of dipole parametrizations that the whole Q^2 dependence is constrained by the low- Q^2 behavior is not justified by QCD. Nevertheless, given the insufficient knowledge available about the strange FF of the nucleon, the adopted dipole parametrization suffices for the present exploratory study.

q	g_A^q	m_{Aq} [GeV]
u	0.859(18)	1.187(65)
d	-0.423(17)	1.168(54)
s	-0.044(8)	0.992(164)

TABLE I. Parameters of the flavor decomposition of the nucleon axial form factor according to Ref. [63].

A priori, no conclusive bounds are available from experiments for any of these parameters [59]. On the other hand, significant progress has been made in the determination of nucleon properties on the lattice in the past few years (see for instance the FLAG review [61]). We adopt the numerical values of these parameters obtained in Ref [62] by the Extended Twisted Mass (ETM) Collaboration: $\mu_s = -0.017(4)$, $\langle r_M^2 \rangle^s = -0.015(9) \text{ fm}^2$ and $\langle r_E^2 \rangle^s = 0.0048(6) \text{ fm}^2$.

Because of its interest in neutrino physics, the isovector axial FF has received considerable attention from LQCD practitioners, and several determinations have become available [34]. However, as shown in Eq. (11), in presence of NSI more input from QCD is required. The flavor decomposition of the axial current

$$\langle N | \bar{q} \gamma^\mu \gamma_5 q | N \rangle \equiv \bar{u}(p') \left[F_A^q(Q^2) \gamma^\mu \gamma_5 + \frac{F_P^q(Q^2)}{M} q^\mu \gamma_5 \right] u(p), \quad (18)$$

with $q = u, d, s$, performed also by the ETM collaboration [63] is well suited for our purposes. They provide dipole parametrizations

$$F_A^q(Q^2) = g_A^q \left(1 + \frac{Q^2}{m_{Aq}^2} \right)^{-2}. \quad (19)$$

Couplings g_A^q and axial masses m_{Aq}^2 from Ref. [63] are compiled in Table I. It is then straightforward to find

$$\begin{aligned} F_A^{iv}(Q^2) &= F_A^u(Q^2) - F_A^d(Q^2) \\ F_A^{is}(Q^2) &= F_A^u(Q^2) + F_A^d(Q^2). \end{aligned} \quad (20)$$

D. NSI couplings

In the present study, NSI couplings are assumed to be real, disregarding CP (or T) violation [64]. Furthermore, we restrict ourselves to the flavor diagonal case and focus on muon (anti)neutrinos, which represent the dominant fraction in accelerator beams. Finally, we can safely neglect NSI couplings to strange quarks, for which there are no bounds at present. Besides being small, these ϵ_{ij}^{sX} appear always multiplied by the strange FF of the nucleon which are also quite small.

All in all, we are left with $\epsilon_{\mu\mu}^{uV,dV}$ and $\epsilon_{\mu\mu}^{uA,dA}$; 90% confidence level (CL) intervals have been obtained from the analysis of atmospheric neutrino oscillations at Super-Kamiokande and high energy scattering data taken at

NuTeV [22] and are given in Table II. In the absence of information about the correlation matrices, we treat them as uncorrelated.

NSI Couplings	90% CL interval	NSI Couplings	90% CL interval
$\epsilon_{\mu\mu}^{uV}$	[-0.044,0.044]	$\epsilon_{\mu\mu}^{uA}$	[-0.094,0.14]
$\epsilon_{\mu\mu}^{dV}$	[-0.042,0.042]	$\epsilon_{\mu\mu}^{dA}$	[-0.072,0.057]

TABLE II. Neutral current flavor diagonal vector and axial neutrino-quark NSI couplings taken from Refs. [12, 22].

E. Spin Density Matrix

After the neutrino-nucleon interaction, the polarization state of the outgoing nucleon is characterized by its spin density matrix [54, 55, 65]:

$$\rho_f(p') = \mathcal{L}^{\mu\nu} \Lambda(p') \Gamma_\mu \rho(p) \tilde{\Gamma}_\nu \Lambda(p'), \quad (21)$$

where $\tilde{\Gamma}_\nu = \gamma^0 \Gamma_\nu^\dagger \gamma^0$, with Γ_ν introduced in Eq. (10), and $\Lambda(p) \equiv \not{p} + M$. The leptonic tensor, obtained from the currents in Eqs. (7,8) is

$$\mathcal{L}^{\mu\nu} = \text{Tr}[\gamma^\mu (1 \mp \gamma_5) \not{k} \gamma^\nu (1 \mp \gamma_5) \not{k}'], \quad (22)$$

where the upper (lower) sign is for neutrinos (anti-neutrinos). Assuming that the initial nucleon is unpolarized

$$\rho(p) = \frac{1}{2} \Lambda(p) \quad (23)$$

F. Differential cross section

The differential cross section for the process in (5) is given by

$$\frac{d\sigma}{dQ^2} = \frac{1}{64\pi M^2 E_\nu^2} \overline{\sum} \sum |\mathcal{M}|^2 \quad (24)$$

where E_ν is the incoming (anti)neutrino energy in the Laboratory frame (LAB). The scattering amplitude of Eq. (6) squared is summed over the final nucleon spins and averaged over the initial ones:

$$\overline{\sum} \sum |\mathcal{M}|^2 = \frac{G_F^2}{4} \mathcal{L}^{\mu\nu} \mathcal{J}_{\mu\nu} \quad (25)$$

The hadronic tensor $\mathcal{J}_{\mu\nu}$ is written with the help of Eqs. (9,10) as,

$$\mathcal{J}_{\mu\nu} = \text{Tr} \left[\Gamma_\mu \Lambda(p) \tilde{\Gamma}_\nu \Lambda(p') \right]. \quad (26)$$

Using the identity

$$\Lambda(p') \Lambda(p') = 2M \Lambda(p'), \quad (27)$$

$\mathcal{J}_{\mu\nu}$ can be recast as

$$\begin{aligned}\mathcal{J}_{\mu\nu} &= \frac{1}{2M} \mathbf{Tr} \left[\Lambda(p') \Gamma_\mu \Lambda(p) \tilde{\Gamma}_\nu \Lambda(p') \right] \\ &= \frac{1}{M} \mathbf{Tr} \left[\Lambda(p') \Gamma_\mu \rho(p) \tilde{\Gamma}_\nu \Lambda(p') \right].\end{aligned}\quad (28)$$

Therefore,

$$\mathcal{L}^{\mu\nu} \mathcal{J}_{\mu\nu} = \frac{1}{M} \mathbf{Tr} [\rho_f(p')] \equiv 64M^2 E_\nu^2 \mathcal{N}. \quad (29)$$

G. Final-nucleon polarization

The polarization 4-vector for the final nucleon corresponding to reaction (5) can be written in terms of the spin density matrix as [54, 55, 65]:

$$\zeta^\tau = \frac{\mathbf{Tr}[\gamma^\tau \gamma_5 \rho_f(p')]}{\mathbf{Tr}[\rho_f(p')]} = \frac{\mathcal{L}^{\alpha\beta} \mathbf{Tr}[\gamma^\tau \gamma_5 \Lambda(p') \Gamma_\alpha \Lambda(p) \tilde{\Gamma}_\beta \Lambda(p')]}{\mathcal{L}^{\alpha\beta} \mathbf{Tr}[\Lambda(p') \Gamma_\alpha \Lambda(p) \tilde{\Gamma}_\beta \Lambda(p')]} \quad (30)$$

We then rely on the identities,

$$\Lambda(p') \gamma^\tau \gamma_5 \Lambda(p') = 2M \left(g^{\tau\sigma} - \frac{p'^\tau p'^\sigma}{M^2} \right) \Lambda(p') \gamma_\sigma \gamma_5, \quad (31)$$

and Eq. (27) to rewrite Eq. (30) as [54, 55]

$$\zeta^\tau = \left(g^{\tau\sigma} - \frac{p'^\tau p'^\sigma}{M^2} \right) \frac{\mathcal{L}^{\alpha\beta} \mathbf{Tr}[\gamma_\sigma \gamma_5 \Lambda(p') \Gamma_\alpha \Lambda(p) \tilde{\Gamma}_\beta]}{\mathcal{L}^{\alpha\beta} \mathbf{Tr}[\Lambda(p') \Gamma_\alpha \Lambda(p) \tilde{\Gamma}_\beta]}. \quad (32)$$

Using Eq. (32), it is easy to verify that in the rest frame of the final nucleon the polarization vector is purely space-like, i.e. $\zeta^\tau = (0, \vec{\zeta})$. Further, Eq. (32) explicitly shows that $\zeta \cdot p' = 0$.

In the following, we first obtain the polarization 4-vector in LAB, where it is denoted as χ , by evaluating Eq. (32) in that frame. Then, it is expressed in the rest frame of the final nucleon by means of the boost

$$\zeta^\sigma = \Lambda_\tau^\sigma(\vec{\beta} = \vec{p}'/E_{p'}) \chi^\tau, \quad (33)$$

where $E_{p'} = \sqrt{M^2 + \vec{p}'^2}$. The kinematics for the reaction in LAB is depicted in Fig. 1. As the target is unpolarized and the incident particles are polarized along the direction of their momentum, the azimuthal dependence averages out. Therefore, all momenta lie on the scattering plane.

We write the polarization vector ($\vec{\chi}$)⁴ in terms of laboratory variables, spanning it along three basis vectors

defined as:

$$\begin{aligned}\hat{e}_L &= \frac{\vec{p}'}{|\vec{p}'|} \\ \hat{e}_P &= \frac{\vec{p}' \times \vec{k}}{|\vec{p}' \times \vec{k}|} \\ \hat{e}_T &= \hat{e}_L \times \hat{e}_P\end{aligned}\quad (34)$$

In such a basis,

$$\vec{\chi} = \chi_L \hat{e}_L + \chi_T \hat{e}_T + \chi_P \hat{e}_P, \quad (35)$$

where the components along longitudinal, perpendicular and transverse directions are denoted χ_L , χ_P and χ_T , respectively.

Figure 1, illustrates that, while the longitudinal and transverse components lie on the scattering plane, the perpendicular component is orthogonal to the scattering plane. The perpendicular component arises in presence of T violation [66, 67]. In the present study the NSI couplings are taken to be real, so T invariance is respected and $\chi_P = 0$.

In order to extract the components $\chi_{L,T}$ we first write the most general expression for $\vec{\chi}$ using the available vectors:

$$\mathcal{N} \vec{\chi} = \tilde{a}_k \vec{k} + \tilde{a}_{p'} \vec{p}' + \tilde{a}_{k'} \vec{k}' + \tilde{a}_p \vec{p}, \quad (36)$$

where coefficients \tilde{a}_i are Lorentz scalars. In the LAB frame $\vec{p} = 0$ and, hence, the contribution due to \tilde{a}_p is zero. Finally, momentum conservation reduces the number of independent terms by one. Therefore we redefine Eq. (36) as

$$\mathcal{N} \vec{\chi} = a_k \vec{k} + a_{p'} \vec{p}'. \quad (37)$$

Using Eqs. (34)–(37), one can easily obtain

$$\begin{aligned}\chi_L(Q^2) &= \frac{[a_k \vec{k} \cdot \vec{p}' + a_{p'} |\vec{p}'|^2]}{|\vec{p}'| \mathcal{N}} \\ \chi_T(Q^2) &= \frac{a_k [(\vec{k} \cdot \vec{p}')^2 - |\vec{k}|^2 |\vec{p}'|^2]}{\mathcal{N} |\vec{p}'| |\vec{k} \times \vec{p}'|}.\end{aligned}\quad (38)$$

As announced earlier, we use the boost of Eq. (33) to get the polarization vector $\vec{\zeta}$ in the final nucleon's rest frame. As the Lorentz boost is along the direction of \vec{p}' or \hat{e}_L , the transverse component being orthogonal to \hat{e}_L will not be affected, i.e. $\zeta_T = \chi_T$. In the longitudinal direction, we have

$$\chi_L = \gamma(\zeta_L - \beta \zeta_0)$$

where $\gamma = E_{p'}/M$ and $\zeta_0 = 0$. Therefore the final expressions for polarization components in the rest frame of the final nucleon, given in the basis of Eq. (34) read as:

$$\begin{aligned}\zeta_L(Q^2) &= \frac{M}{E_{p'}} [a_k \vec{k} \cdot \vec{p}' + a_{p'} |\vec{p}'|^2] \frac{1}{|\vec{p}'| \mathcal{N}} \\ \zeta_T(Q^2) &= \frac{a_k [(\vec{k} \cdot \vec{p}')^2 - |\vec{k}|^2 |\vec{p}'|^2]}{\mathcal{N} |\vec{p}'| |\vec{k} \times \vec{p}'|}.\end{aligned}\quad (39)$$

⁴ The time component χ^0 can be readily obtained from the orthogonality condition $\chi \cdot p' = 0$.

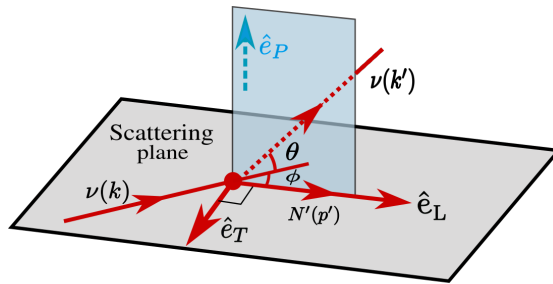


FIG. 1. Kinematics for the NCE process in the laboratory frame, where \hat{e}_L , \hat{e}_P and \hat{e}_T represent longitudinal, perpendicular and transverse directions of the final nucleon polarization vector. Indicated are also the directions of the incoming neutrino and the outgoing neutrino and nucleon, with their corresponding scattering angles θ and ϕ .

The above expression can further be simplified as:

$$\begin{aligned}\mathcal{N}\zeta_L(Q^2) &= \frac{M}{E_{p'}} [a_k E_\nu \cos \phi + a_{p'} |\vec{p}'] \\ \mathcal{N}\zeta_T(Q^2) &= -a_k E_\nu \sin \phi,\end{aligned}\quad (40)$$

where we have used that $E_\nu = |\vec{k}|$; ϕ is the scattering angle of the final nucleon with respect to the incident (anti)neutrino in the LAB frame (see Fig. 1).

Explicit expressions for $\zeta_{L,T}$, along with the coefficients $a_{k,p'}$ and \mathcal{N} , are given in Appendix B in terms of the ϵ_{ij}^{fX} -dependent FF of Eq. (11). Additionally, the ratio of transverse to longitudinal polarization is obtained and is given in Eq. (A10). Such a ratio might be experimentally convenient because it entails the cancellation of some systematic uncertainties.

III. RESULTS

The NC vector and axial FF, $\tilde{F}_{1,2,A}^{p,n}$ introduced in Eq. (11) are shown in Fig. 2. The solid green (red) line represents the SM results with (without) strangeness. The shaded regions depict the possible deviations due to NSI within the 90% CL intervals of Table II. It is apparent that, according to the ETM determination of Refs. [62, 63], the impact of strangeness is small compared to the NSI band. Because of the accidental cancellation among terms in the $(1/2 - 2s_w^2)$ factor, \tilde{F}_1^p is small in the SM and the possible NSI contribution is relatively large.

Next, we compute the total (integrated) cross-sections for the processes given in Eq. (5) to investigate the effects of NSI. The results are shown in Fig. 3. The black solid lines are obtained in the SM, including both vector and axial strange FF, while the blue-shaded region gives the possible deviation due to NSI. The cross sections are displayed for incident muon neutrinos and antineutrinos, as well as for protons and neutron targets. The latter would only be experimentally accessible with deuteron targets. In this case, the presence of an additional nucleon would introduce moderate but QCD dependent corrections [68, 69]. One notices that, given the

current bounds, NSI might cause a significant deviation with respect to the SM cross section. For example, at a (anti)neutrino energy of 5 GeV, the maximal variation for the neutron target is around 20%, while for the proton target, it goes as high as 35% when compared with the SM predictions. The similar study performed earlier [31] was, to the best of our knowledge, the first to investigate the impact of FSI in the NCE $(\bar{\nu})$ -nucleon scattering cross section. However, as mentioned after Eq. 11, an ad-hoc Q^2 FF was assumed and the isoscalar FF, F_A^{iso} , was also not considered.

Further insight can be gained from differential cross sections. In Fig. 4, we plot the Q^2 dependence of $d\sigma/dQ^2$ at two representative (anti)neutrino energies, $E_\nu = 1$ and 3 GeV. NSI can considerably shift the maximum value of $d\sigma/dQ^2$, although measurements at low Q^2 , where such a maximum is reached, entail experimental difficulties due to the small nucleon recoil. This is also the region where deuteron corrections are more pronounced. The plots reflect the known fact that $d\sigma/dQ^2(Q^2 = 0)$ is E_ν independent and the same for neutrinos and antineutrinos. See for instance Eqs. (12,16,18) of Ref. [70], whose generalization to the case of non-zero NSI using Eq. (11) is straightforward. On the other hand, the target dependence is apparent. At $Q^2 = 0$, a departure from SM of up to +40(−25)% is found for the proton target due to NSI, while it is around 20% for the neutron target.

Additional information on the impact of NSI can be obtained from the polarization of the outgoing nucleon. We use Eq. (39), to obtain the Q^2 dependence of longitudinal (ζ_L) and transverse (ζ_T) polarization. The explicit expressions for $\zeta_{L,T}$ are given in Appendix B. The results are shown in Figs. 5 and 6 for a representative (anti)neutrino energy of 1 GeV.

In the case of longitudinal (ζ_L) polarization it is noteworthy that distinct behaviors are observed for both neutrinos and antineutrinos. The variation due to NSI is nearly negligible close to both low and high Q^2 thresholds, but a significant variation is evident at intermediate values of Q^2 , particularly for antineutrino scattering. At low Q^2 , the outgoing nucleon's longitudinal polarization is almost zero and, as Q^2 increases, it approaches -1 (1)

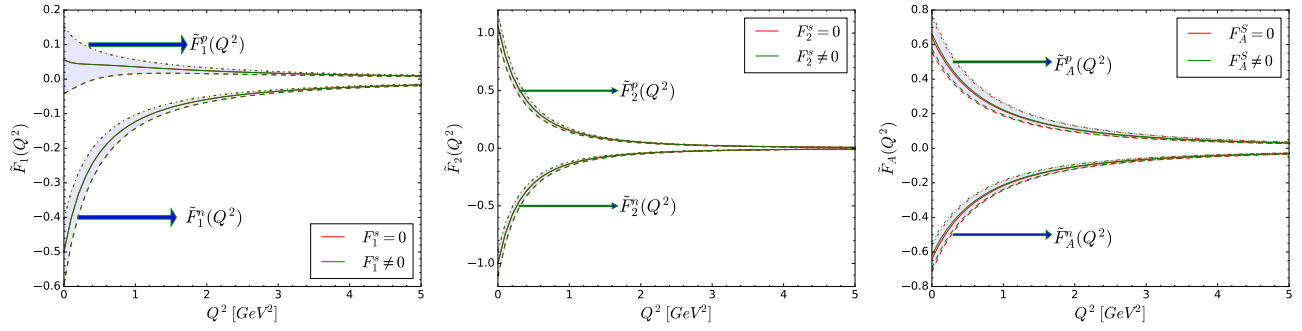


FIG. 2. The vector and axial NC form factors defined in Eq. (11) are plotted as a function of Q^2 . Solid lines correspond to the SM. The grey bands limited by dashed lines from below and dash-dotted lines from above display the NSI deviations within the 90% CL intervals of Table II. The green (red) line represents results with (without) strangeness.

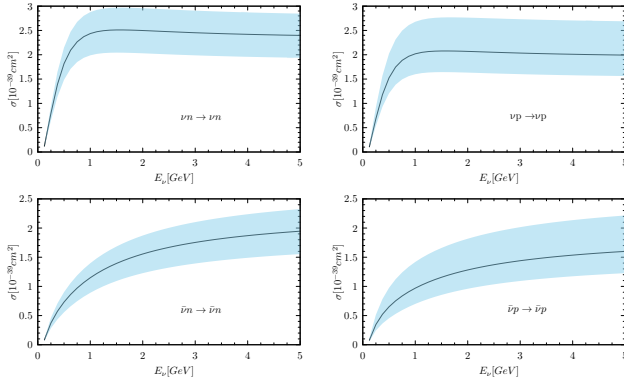


FIG. 3. Total cross section for NC (anti)neutrino elastic scattering as a function of E_ν . The black solid lines represent the SM results while the shaded bands show the deviations by NSI within the 90% CL intervals in Table II.

for the neutrino (antineutrino) channel.⁵

On the other hand, in the SM, the transverse component of polarization of the outgoing proton (ζ_T) is small at $Q^2 \sim 0$ and goes to zero quite rapidly. We find that NSI bring significant deviations, specially at low Q^2 . Meanwhile, neutrons are found to be largely polarized in the transverse direction at low Q^2 , while this transverse component gradually reaches zero with increasing Q^2 . Similar findings were observed previously in Ref. [55]. The NSI band appears broader for antineutrinos at middle Q^2 ranges.

IV. SUMMARY AND CONCLUSIONS

We have studied (anti)neutrino-nucleon NC elastic scattering in presence of NSI of SM neutrinos with light (u, d, s) quarks. Assuming a heavy mediator, these interactions take the well-known form of four-fermion vertices, where the new physics is concealed in the NSI couplings. We have therefore derived the NC matrix elements of the nucleon with NSI, writing them in terms of vector and axial FF, which encode the strong-interaction physics. We find that in presence of NSI, these matrix elements depend not only on the axial isovector FF but also on the isoscalar one, absent in the SM weak interactions. For this reason, for our numerical predictions we rely on the flavor decomposition of the axial FF published by the ETM LQCD collaboration [63]. Under the assumption that there is no significant new physics in electron-nucleon scattering, vector FF can be safely obtained from electron scattering (corrected by radiative corrections). We adopt this strategy for the vector isovector and isoscalar FF but rely on the ETM determination [62] of the strange electromagnetic FF.

In our evaluation of scattering observables, only the muon flavor, with flavor-diagonal, T -conserving interactions have been considered. In this scenario there are four non-zero real couplings $\epsilon_{\mu\mu}^{uV,dV}$ and $\epsilon_{\mu\mu}^{uA,dA}$, for which confidence intervals had been obtained from oscillation and deep-inelastic scattering measurements [22]. For such ranges, we find a significant presence of NSI in differential and integrated NC (anti)neutrino-nucleon cross sections, particularly for a proton target and at low Q^2 . For this choice of target and kinematics, NSI have a large impact on the polarization of the outgoing nucleons, especially in the transverse direction.

Neutrino scattering experiments on hydrogen and deuterium are notoriously challenging. So far, modern neutrino experiments have chosen heavy targets to maximize statistics. Nevertheless, (anti)neutrino-nucleon interactions are not only a key ingredient and a source of uncertainties in theoretical models of (anti)neutrino-nucleon cross sections but are interesting by themselves [35]. The

⁵ We note the different sign of our SM results for the nucleon longitudinal polarization compared to the ones of Ref. [55] (for $\bar{\nu}$ scattering). It is worth stressing that at the largest Q^2 , corresponding to backward scattering, the value of ζ_L is constrained to be -1 (1) for $\nu(\bar{\nu})$ by the conservation of the spin projection along the direction of motion.

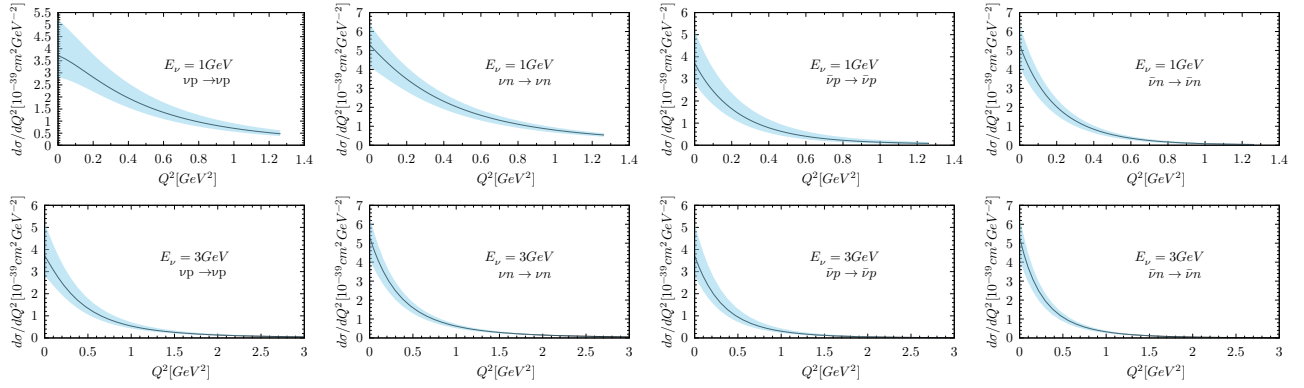


FIG. 4. Differential cross section with respect to Q^2 for NCE channels at $E_\nu = 1$ GeV (top) and 3 GeV (bottom). Lines and bands have the same meaning as in Fig. 3.

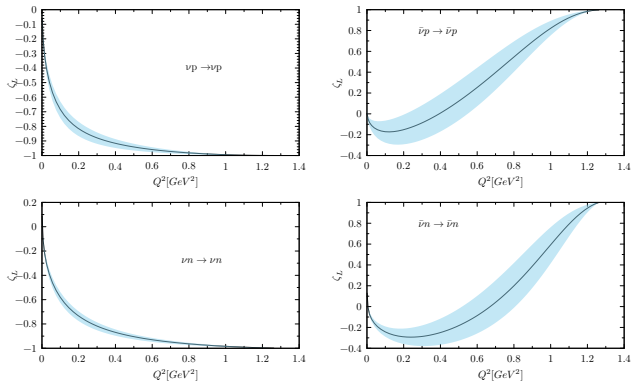


FIG. 5. Q^2 distribution of the longitudinal polarization of the outgoing nucleon, ζ_L for the NCE channels at $E_\nu = 1$ GeV. Lines and bands have the same meaning as in Fig. 4.

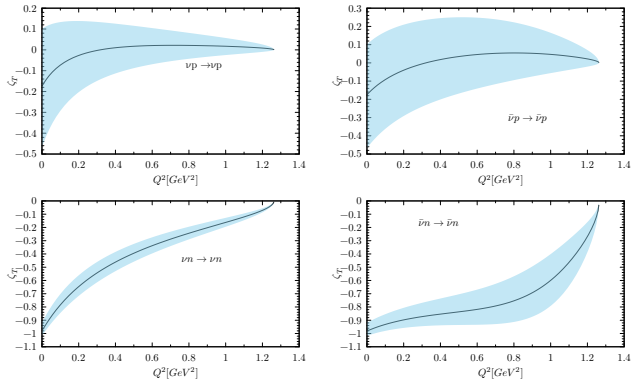


FIG. 6. Q^2 distribution of the transverse polarization of the outgoing nucleon, ζ_T for the NCE channels at $E_\nu = 1$ GeV. Lines and bands have the same meaning as in Fig. 4.

present study adds to this statement: it shows that, given the current and expected success of LQCD in obtaining nucleon FF, modern measurements of NC (anti)neutrino-nucleon elastic scattering can be instrumental in discovering or constraining non-standard interactions.

ACKNOWLEDGMENTS

One of the authors, Ilma, greatly acknowledges support from the University Grants Commission (UGC), India, for providing the Junior Research Fellowship F.no. 16-9 (June 2019)/2019 (NET/CSIR). This work has been also partially supported by the Spanish Ministry of Science and Innovation under Grants No. PID2020-112777GB-I00 and PID2023-147458NB-C21, funded by MICIU/AEI/10.13039/501100011033, by the EU STRONG-2020 project under the program H2020-INFRAIA-2018-1, grant agreement no. 82409, by Generalitat Valenciana grant CIPROM/2023/59, and by the ‘‘Planes Complementarios de I+D+i’’ program (grant ASFAE/2022/022) by MICIU with funding from the European Union NextGenerationEU and Generalitat Valenciana. IRS also acknowledges support from the Junta de Andalucia (Grant No. FQM-225).

APPENDICES

A. Nucleon electromagnetic form factors

The electromagnetic FF $F_{1,2}^{p,n}(Q^2)$ appearing in Eq. (11) are generally expressed in terms of Sach’s electric $G_E^{p,n}(Q^2)$ and magnetic $G_M^{p,n}(Q^2)$ FF as:

$$F_1^N(Q^2) = \frac{G_E^N(Q^2) + \tau G_M^N(Q^2)}{1 + \tau}$$

$$F_2^N(Q^2) = \frac{G_M^N(Q^2) - G_E^N(Q^2)}{1 + \tau} \quad ; \quad N = n, p, \quad (\text{A1})$$

with $\tau = Q^2/4M^2$. For the latter we rely on the parametrization by Galster et al. [71]:

$$\begin{aligned} G_E^p &= \left(\frac{1}{1 + Q^2/M_V^2} \right)^2 \\ &= \frac{G_M^p}{\mu_p} = \frac{G_M^n}{\mu_n} \\ &= -(1 + \lambda_n \tau) \frac{G_E^n}{\mu_n \tau} \end{aligned} \quad (\text{A2})$$

where $M_V = 0.843$ GeV, $\mu_p = 2.792847$, $\mu_n = -1.913043$, and $\lambda_n = 5.6$.

B. Final nucleon polarization in terms of form factors

Besides the incident energy, E_ν , there is only one independent kinematic variable. We choose Q^2 as such a variable but, for the sake of compactness, in the following expressions we use dimensionless variables

$$\begin{aligned} \tau &\equiv \frac{Q^2}{4M^2} \\ y &\equiv \frac{p \cdot q}{p \cdot k} = \frac{Q^2}{2ME_\nu}. \end{aligned} \quad (\text{A3})$$

The contraction of the leptonic and hadronic tensors, \mathcal{N} of Eq. (29), is then expressed as:

$$\begin{aligned} \mathcal{N} &= 2(1-y) \left(\tilde{F}_A^2 + \frac{\tau \tilde{G}_M^2 + \tilde{G}_E^2}{1+\tau} \right) \\ &+ y^2 (\tilde{G}_M \mp \tilde{F}_A)^2 + \frac{My}{E_\nu} \left(\tilde{F}_A^2 - \frac{\tau \tilde{G}_M^2 + \tilde{G}_E^2}{1+\tau} \right) \\ &\pm 4y \tilde{G}_M \tilde{F}_A. \end{aligned} \quad (\text{A4})$$

where (lower)upper sign is for (anti)neutrinos. Equation (A1) has been used to revert $\tilde{F}_{1,2}$ in terms of $\tilde{G}_{E,M}$.

The coefficients $a_{k,p'}$ of Eq (37) in terms of these variables are written as:

$$a_k = \frac{\tilde{G}_E y}{M\tau} \left[\pm \tilde{G}_M y + \tilde{F}_A (2-y) \right] \quad (\text{A5})$$

$$\begin{aligned} a_{p'} &= \frac{1}{2M\tau(\tau+1)} \left[\tilde{F}_A \tilde{G}_E (y-2)(2\tau+y) - \tilde{F}_A \tilde{G}_M \right. \\ &\times (2\tau+1)(y^2 + 2\tau((y-2)y+2)) \\ &\mp \left(\tilde{G}_E \tilde{G}_M y (2\tau+y) - (2\tau+1)(y-2)y \right. \\ &\left. \left. \times (\tilde{F}_A^2(\tau+1) + \tilde{G}_M^2 \tau) \right) \right]. \end{aligned} \quad (\text{A6})$$

Substituting them in Eq. (40) one obtains for the polarization vector components along the two orthogonal directions i.e. transverse (ζ_T) and longitudinal (ζ_L):

$$\mathcal{N} \zeta_T = -2 \sin \phi [\pm y \tilde{G}_M + (2-y) \tilde{F}_A] \tilde{G}_E \quad (\text{A7})$$

$$\begin{aligned} \mathcal{N} \zeta_L &= -\frac{q_0}{|\vec{q}|} [\pm y \tilde{G}_M + (2-y) \tilde{F}_A] \\ &\left[(2-y) \tilde{G}_M \pm y \left(\frac{1+\tau}{\tau} \right) \tilde{F}_A \right]. \end{aligned} \quad (\text{A8})$$

The sinus of the outgoing-nucleon's scattering angle in LAB, with respect to the incoming (anti)neutrino direction can be expressed as

$$\sin \phi = \sqrt{\frac{4\tau(1-y) - y^2}{4\tau(1+\tau)}}. \quad (\text{A9})$$

Finally, the ratio of transverse to longitudinal polarization is given by

$$\frac{\zeta_T}{\zeta_L} = \frac{|\vec{q}| \sin \phi}{M} \frac{\tilde{G}_E}{\left[\tau(2-y) \tilde{G}_M \pm y(1+\tau) \tilde{F}_A \right]}. \quad (\text{A10})$$

-
- [1] S. Weinberg, *Phys.Rev.Lett.* **19**, 1264 (1967).
[2] R. L. Workman *et al.* (Particle Data Group), *PTEP* **2022**, 083C01 (2022).
[3] M. Lindner, W. Rodejohann, and X.-J. Xu, *JHEP* **03**, 097 (2017), [arXiv:1612.04150 \[hep-ph\]](#).
[4] I. Bischer and W. Rodejohann, *Nucl. Phys. B* **947**, 114746 (2019), [arXiv:1905.08699 \[hep-ph\]](#).
[5] T. Han, J. Liao, H. Liu, and D. Marfatia, *JHEP* **07**, 207 (2020), [arXiv:2004.13869 \[hep-ph\]](#).
[6] Y. Du, H.-L. Li, J. Tang, S. Vihonen, and J.-H. Yu, *Phys. Rev. D* **105**, 075022 (2022), [arXiv:2106.15800 \[hep-ph\]](#).
[7] L. Wolfenstein, *Phys.Rev.D* **17**, 2369 (1978).
[8] Y. Grossman, *Phys.Lett.B* **359**, 141 (1995), [arXiv:hep-ph/9507344 \[hep-ph\]](#).
[9] Z. Berezhiani and A. Rossi, *Phys.Lett.B* **535**, 207 (2002), [arXiv:hep-ph/0111137 \[hep-ph\]](#).
[10] S. Davidson, C. Pena-Garay, N. Rius, and A. Santamaria, *JHEP* **03**, 011 (2003), [arXiv:hep-ph/0302093 \[hep-ph\]](#).
[11] T. Ohlsson, *Rept.Prog.Phys.* **76**, 044201 (2013), [arXiv:1209.2710 \[hep-ph\]](#).
[12] Y. Farzan and M. Tortola, *Front.in Phys.* **6**, 10 (2018), [arXiv:1710.09360 \[hep-ph\]](#).
[13] M. Masud, A. Chatterjee, and P. Mehta, *J.Phys.G* **43**, 095005 (2016), [arXiv:1510.08261 \[hep-ph\]](#).
[14] A. de Gouvêa and K. J. Kelly, *Nucl.Phys.B* **908**, 13658 (2016), [arXiv:1511.05562 \[hep-ph\]](#).
[15] D. V. Forero and P. Huber, *Phys.Rev.Lett.* **117**, 031801 (2016), [arXiv:1601.03736 \[hep-ph\]](#).
[16] I. Esteban, M. Gonzalez-Garcia, and M. Maltoni, *JHEP* **06**, 055 (2019), [arXiv:1905.05203 \[hep-ph\]](#).
[17] F. Capozzi, S. S. Chatterjee, and A. Palazzo,

- Phys.Rev.Lett. **124**, 111801 (2020), arXiv:1908.06992 [hep-ph].
- [18] J. Barranco, O. Miranda, C. Moura, and J. Valle, Phys.Rev.D **77**, 093014 (2008), arXiv:0711.0698 [hep-ph].
- [19] D. Forero and M. Guzzo, Phys.Rev.D **84**, 013002 (2011).
- [20] A. N. Khan, D. W. McKay, and F. Tahir, Phys.Rev.D **90**, 053008 (2014), arXiv:1407.4263 [hep-ph].
- [21] F. Escrihuela, L. Flores, O. Miranda, and J. Rendón, JHEP **07**, 061 (2021), arXiv:2105.06484 [hep-ph].
- [22] F. Escrihuela, M. Tortola, J. Valle, and O. Miranda, Phys.Rev.D **83**, 093002 (2011), arXiv:1103.1366 [hep-ph].
- [23] D. Akimov *et al.* (COHERENT), Science **357**, 1123 (2017), arXiv:1708.01294 [nucl-ex].
- [24] P. Coloma, M. Gonzalez-Garcia, M. Maltoni, and T. Schwetz, Phys.Rev.D **96**, 115007 (2017), arXiv:1708.02899 [hep-ph].
- [25] J. Liao and D. Marfatia, Phys.Lett.B **775**, 54 (2017), arXiv:1708.04255 [hep-ph].
- [26] D. Aristizabal Sierra, V. De Romeri, and N. Rojas, Phys.Rev.D **98**, 075018 (2018), arXiv:1806.07424 [hep-ph].
- [27] P. B. Denton and J. Gehrlein, JHEP **04**, 266 (2021), arXiv:2008.06062 [hep-ph].
- [28] A. N. Khan, D. W. McKay, and W. Rodejohann, Phys.Rev.D **104**, 015019 (2021), arXiv:2104.00425 [hep-ph].
- [29] L. Flores, N. Nath, and E. Peinado, Phys.Rev.D **105**, 055010 (2022), arXiv:2112.05103 [hep-ph].
- [30] V. De Romeri *et al.*, JHEP **04**, 035 (2023), arXiv:2211.11905 [hep-ph].
- [31] D. Papoulias and T. Kosmas, Adv.High Energy Phys. **2016**, 1490860 (2016), arXiv:1611.05069 [hep-ph].
- [32] K. Borah, M. Betancourt, R. J. Hill, T. Junk, and O. Tomalak, Phys.Rev.D **110**, 013004 (2024), arXiv:2403.04687 [hep-ph].
- [33] O. Tomalak, M. Betancourt, K. Borah, R. J. Hill, and T. Junk, Phys.Lett.B **854**, 138718 (2024), arXiv:2402.14115 [hep-ph].
- [34] A. S. Meyer, A. Walker-Loud, and C. Wilkinson, Ann.Rev.Nucl.Part.Sci. **72**, 205 (2022), arXiv:2201.01839 [hep-lat].
- [35] L. Alvarez-Ruso *et al.* (2022) arXiv:2203.11298 [hep-ex].
- [36] H. Duyang, B. Guo, S. Mishra, and R. Petti, Eur.Phys.J.Plus **139**, 1014 (2024).
- [37] T. Cai *et al.* (MINERvA), Nature **614**, 48 (2023).
- [38] J. Kopp, N. Rocco, and Z. Tabrizi, JHEP **08**, 187 (2024), arXiv:2401.07902 [hep-ph].
- [39] Y.-R. Kong *et al.*, Phys.Rev.D **108**, 095036 (2023), arXiv:2307.07239 [hep-ph].
- [40] K. Hagiwara, K. Mawatari, and H. Yokoya, Nucl.Phys.B **668**, 364 (2003), [Erratum: Nucl.Phys.B 701, 405–406 (2004)], arXiv:hep-ph/0305324 [hep-ph].
- [41] K. M. Graczyk, Nucl.Phys.A **748**, 313 (2005), arXiv:hep-ph/0407275 [hep-ph].
- [42] K. S. Kuzmin, V. V. Lyubushkin, and V. A. Naumov (2005) pp. 154–157, arXiv:hep-ph/0408107 [hep-ph].
- [43] K. S. Kuzmin, V. V. Lyubushkin, and V. A. Naumov (2005) pp. 158–161, arXiv:hep-ph/0408106 [hep-ph].
- [44] M. Valverde, J. E. Amaro, J. Nieves, and C. Maieron, Phys.Lett.B **642**, 218 (2006), arXiv:nucl-th/0606042 [nucl-th].
- [45] J. Sobczyk, N. Rocco, and J. Nieves, Phys.Rev.C **100**, 035501 (2019), arXiv:1906.05656 [nucl-th].
- [46] A. Fatima, M. Sajjad Athar, and S. Singh, Phys.Rev.D **102**, 113009 (2020), arXiv:2010.10311 [hep-ph].
- [47] E. Hernández, J. Nieves, F. Sánchez, and J. Sobczyk, Phys.Lett.B **829**, 137046 (2022), arXiv:2202.07539 [hep-ph].
- [48] J. Isaacson, S. Höche, F. Siegert, and S. Wang, Phys.Rev.D **108**, 093004 (2023), arXiv:2303.08104 [hep-ph].
- [49] Z. Li *et al.* (Super-Kamiokande), Phys. Rev. D **98**, 052006 (2018), arXiv:1711.09436 [hep-ex].
- [50] F. Akbar, M. Rafi Alam, M. Sajjad Athar, and S. Singh, Phys.Rev.D **94**, 114031 (2016), arXiv:1608.02103 [hep-ph].
- [51] A. Fatima, M. Sajjad Athar, and S. Singh, Phys.Rev.D **98**, 033005 (2018), arXiv:1806.08597 [hep-ph].
- [52] K. M. Graczyk and B. E. Kowal, Phys.Rev.D **104**, 033005 (2021), arXiv:2106.11383 [hep-ph].
- [53] K. M. Graczyk and B. E. Kowal, Phys.Rev.D **108**, 093002 (2023), arXiv:2307.00661 [hep-ph].
- [54] S. M. Bilenky and E. Christova, J.Phys.G **40**, 075004 (2013), arXiv:1303.3710 [hep-ph].
- [55] S. Bilenky and E. Christova, Phys.Part.Nucl.Lett. **10**, 651 (2013), arXiv:1307.7275 [hep-ph].
- [56] O. Miranda and H. Nunokawa, New J.Phys. **17**, 095002 (2015), arXiv:1505.06254 [hep-ph].
- [57] O. Tomalak, Q. Chen, R. J. Hill, and K. S. McFarland, Nature Commun. **13**, 5286 (2022), arXiv:2105.07939 [hep-ph].
- [58] O. Tomalak, Q. Chen, R. J. Hill, K. S. McFarland, and C. Wret, Phys.Rev.D **106**, 093006 (2022), arXiv:2204.11379 [hep-ph].
- [59] F. Maas and K. Paschke, Prog.Part.Nucl.Phys. **95**, 209 (2017).
- [60] G. Garvey, W. Louis, and D. White, Phys.Rev.C **48**, 761 (1993).
- [61] Y. Aoki *et al.* (Flavour Lattice Averaging Group (FLAG)), Eur. Phys. J. C **82**, 869 (2022), arXiv:2111.09849 [hep-lat].
- [62] C. Alexandrou *et al.*, Phys.Rev.D **101**, 031501 (2020), arXiv:1909.10744 [hep-lat].
- [63] C. Alexandrou *et al.*, Phys.Rev.D **104**, 074503 (2021), arXiv:2106.13468 [hep-lat].
- [64] N. Cabibbo, Phys.Lett. **12**, 137 (1964).
- [65] S. M. Bilenky, (1995).
- [66] A. Fatima, M. Sajjad Athar, and S. Singh, Eur.Phys.J.A **54**, 95 (2018), arXiv:1802.04469 [hep-ph].
- [67] M. Sajjad Athar, A. Fatima, and S. Singh, Prog.Part.Nucl.Phys. **129**, 104019 (2023), arXiv:2206.13792 [hep-ph].
- [68] S. Singh and H. Arenhovel (1986) pp. 347–354.
- [69] G. Shen, L. Marcucci, J. Carlson, S. Gandolfi, and R. Schiavilla, Phys.Rev.C **86**, 035503 (2012), arXiv:1205.4337 [nucl-th].
- [70] L. Alvarez-Ruso, Y. Hayato, and J. Nieves, New J.Phys. **16**, 075015 (2014), arXiv:1403.2673 [hep-ph].
- [71] S. Galster *et al.*, Nucl.Phys.B **32**, 221 (1971).